Available online at www.sciencedirect.com
SCIENCE DIRECT®
ELSEVIER
International Journal of Solids and Structures 42 (2005) 4494–4513
INTERNATIONAL JOURNAL OF SOLIDS and STRUCTURES
www.elsevier.com/locate/ijsolstr

Nondestructive damage detection in structures using changes in compliance

Sanghyun Choi [a], Sooyong Park [b,*], Norris Stubbs [c]

[a] *Structural Systems and Site Evaluation Department, Korea Institute of Nuclear Safety, Guseong-Dong, Yuseong-Gu, Daejeon 305-600, South Korea*
[b] *School of Architecture, Youngsan University, San 150 Junam-Ri, Ungsang-Up, Yangsan-Si, Kyungnam 626-847, South Korea*
[c] *Department of Civil Engineering, Texas A&M University, College Station, TX 77843, USA*

Received 20 May 2003; received in revised form 19 December 2004
Available online 12 February 2005

Abstract

A methodology to identify damage in a structure is presented in this paper. The method utilizes a new form of damage index based on the changes in the distribution of the compliance of the structure due to damage. The changes in the compliance distribution are obtained using the mode shapes of the pre-damaged and the post-damaged state of the structure. The validity of the method is demonstrated using numerically generated data from beam structures and experimental data from a free–free beam structure with inflicted damage. In the numerical and experimental examples, the damage identification performance of the proposed method is compared with that of the existing strain-energy-based method. The results of the numerical and experimental studies indicate that the proposed compliance-based damage index method can be used in damage identification of the structure.

Keywords: Damage identification; Compliance; Modal parameters

1. Introduction

Preventing deterioration while maintaining the serviceability of structures has emerged as a prominent problem in structural engineering. To date, numerous nondestructive damage detection (NDD) methods have been proposed and developed using various experimental and theoretical techniques. Some of the

* Corresponding author. Tel.: +82 55 380 9495; fax: +82 55 380 9229/9249.
E-mail addresses: schoi@kins.re.kr (S. Choi), sypark@ysu.ac.kr (S. Park), n-stubbs@tamu.edu (N. Stubbs).

0020-7683/$ - see front matter © 2005 Elsevier Ltd. All rights reserved.
doi:10.1016/j.ijsolstr.2004.12.017

well-known experimental techniques include ultrasonics, radiography, magnetic particle, dye penetrant, and eddy current (Askeland, 1994). These techniques have been applied to small-scale systems and a specific portion of large-scale structures. However, since these "local" methods can only be applied to the detection of damage on a local scale and to accessible portions of the structure, alternative methods that can be applied to the entire structure, the so-called global NDD methods, are gaining acceptance. Two established global methods include thermography and acoustic emission. However, in the past two decades global methods using the dynamic response of a structure have been gaining significant attention. The basic idea behind these vibration-based global methods is that changes in the physical properties of a structural system alter the dynamic response characteristics of the structure.

Early researchers have focused on the relationship between damage (i.e., stiffness loss) and resonant frequency changes (Vandiver, 1977; Gudmundson, 1982). However, even though the resonant frequency changes have been shown to be useful in damage detection problems in mechanical systems with a few degrees of freedom, to determine the location of damage in realistic structures such as offshore platforms and bridges using only frequencies is not practical (Pandey and Biswas, 1994). Frequency change depends on the square root of the stiffness change and the environmental conditions such as temperature and moisture content can easily alter the resonant frequencies of a structure. To overcome these drawbacks, some researchers have focused on utilizing mode shape measures to evaluate damage (Pandey and Biswas, 1994; Rizos et al., 1990). A detailed literature review of vibration-based NDD methods has been provided by Doebling et al. (1996).

To date, numerous vibration-based NDD methods have been presented. However, even though many theories and algorithms have been developed in the field of NDD, up to the present time, no single theory of NDD has been shown to be completely effective in all situations. This may be well observed in a recent round-robin study conducted by Farrar and Jauregui (1996). In that study, the relative performance of prominent vibration-based NDD methods was presented. The methods selected include the changes in flexibility method (Pandey and Biswas, 1994), the mode shape curvature method (Pandey et al., 1991), the change in uniform flexibility shapes curvature method (Zhang and Aktan, 1995), the change in stiffness method (Zimmerman and Kaouk, 1994), and the damage index method (Stubbs et al., 1992). On the basis of 16 damage case studies using numerical and experimental data, even the best-performing algorithm identified in that study, the damage index method, failed to identify two damage locations in two damage cases. Also, recently, Rodriguez (2002) describes the disadvantages in applying prominent vibration-based NDD methods to practical problems in his study. Some of the disadvantages include the requirement of a full modal analysis (e.g., the changes in flexibility method), the need for a full set of modal amplitude readings (e.g., the mode shape curvature method), and no severity estimation scheme (e.g., the change in uniform flexibility shapes curvature method). The authors of this paper recognized that possible solutions to improve the performance of the method could be the development of more effective damage indices.

The objective of this paper is to develop a damage index that is more sensitive to the changes in the vibrational characteristics of a structure and, in turn, improve the damage detectability for the existing damage index method (Stubbs et al., 1992). The stated objective is achieved via the following approach. First, the new damage index, designated the compliance index, which utilizes the changes in the distribution of the compliance of a structure, is developed. The change in the compliance distribution is obtained using the mode shapes of the pre-damaged and the post-damaged structure. Second, the validity of the methodology is demonstrated using simulated modal data from a simple beam and a continuous beam. Finally, the proposed methodology is applied to the experimental data from a free–free beam structure. In the numerical and experimental verifications, the damage prediction results using the compliance index are compared with those using the existing strain-energy-based damage index that performed best in the recent round-robin study (Farrar and Jauregui, 1996).

2. Theory

2.1. The existing strain-energy-based damage index

The damage index method originated from a sensitivity approach that relates changes in modal responses, specifically resonant frequencies, to changes in the mass, damping, and stiffness of a structure (Cawley and Adams, 1979). The damage index method developed by Stubbs et al. (1992) utilizes the change in the modal strain energy distribution due to damage. This method has been corroborated using (1) numerically simulated data for various structural types and classes (Choi and Stubbs, 1997, 2004), (2) experimental modal data generated in a laboratory environment (Kim and Stubbs, 1995), and (3) field data measured on bridge structures (Choi et al., 2004).

The strain-energy-based damage index (will be called the energy index hereafter), β^{e}, for the element j and the eigenmode i is defined as

$$\beta_{ij}^{e} = \frac{k_j}{k_j^*} \approx \frac{\left[\Phi_i^{*\mathrm{T}} C_j \Phi_i^* + \Phi_i^{*\mathrm{T}} K \Phi_i^*\right] \Phi_i^{\mathrm{T}} K \Phi_i}{\left[\Phi_i^{\mathrm{T}} C_j \Phi_i + \Phi_i^{\mathrm{T}} K \Phi_i\right] \Phi_i^{*\mathrm{T}} K \Phi_i^*} \tag{1}$$

where k_j is the stiffness parameter of jth element (EI for a beam member); K is the system stiffness matrix; Φ_i is ith modal vector and the matrix C_j can be obtained from the following relationship:

$$K_j = k_j C_j \tag{2}$$

where K_j is the contribution of the jth element to the system stiffness matrix. Note that in Eq. (1) the superscript asterisk represents the parameter for the post-damaged state of the structure. Note also that the matrix C_j only involves geometric quantities and possibly Poisson's ratio. For NM eigenmodes, the composite form of the energy index is defined as

$$\beta_{j}^{e} = \frac{k_j}{k_j^*} \approx \frac{\sum_{i=1}^{NM}\left[\Phi_i^{*\mathrm{T}} C_j \Phi_i^* + \Phi_i^{*\mathrm{T}} K \Phi_i^*\right] \Phi_i^{\mathrm{T}} K \Phi_i}{\sum_{i=1}^{NM}\left[\Phi_i^{\mathrm{T}} C_j \Phi_i + \Phi_i^{\mathrm{T}} K \Phi_i\right] \Phi_i^{*\mathrm{T}} K \Phi_i^*} \tag{3}$$

Detailed derivation of Eqs. (1) and (3) can be found in the reference (Park et al., 2001).

2.2. The compliance index

The change in the compliance has been applied in the damage identification problem by other researchers (Pandey and Biswas, 1994; Zhang and Aktan, 1995). The existing compliance based methods utilize the change in the measured flexibility matrix estimated from the mass-normalized mode shapes and frequencies. It has been reported that the measured flexibility matrix is most sensitive to changes in the lowest frequency modes of the structure due to the inverse relationship of the square of the modal frequencies (Doebling et al., 1996). Experimental application of these compliance-based method confirmed that the good sensitivity of the modal compliance to structural damage (Pandey and Biswas, 1995; Ko et al., 2002). Also, Lu et al. (2002) have presented the successful application of the compliance-based method to multiple damage location problems.

However, the existing flexibility-based methods can only identify damage locations and no severity estimation schemes are provided since these methods are based on simple comparison between the elements [or the curvatures of the elements] of the compliance matrix of the undamaged structure and those of the damaged structure. No solid relationship between the element-wise compliance change and the obtained modal parameters is given. To overcome the stated drawback, in this paper, the change in the effective compliance of the element is first derived in terms of the modal amplitudes, and the expression for a new damage index

(will be called the compliance index hereafter), which represents the ratio of the compliance of the element before and after damage, is derived.

The general expression for the compliance index may be derived as follows. Using operator notation, the governing equation for an arbitrary continuous structural system (e.g., rod, beam, plate, etc.) may be written as follows:

$$\coprod w = sQ \tag{4}$$

where $\coprod$ is a linear operator; w is a general response of the structure; s is a factor related to the compliance of the structure and Q is a force applied to the structure. Note that Eq. (4) is valid at every point in a structure and the factor, s, represents the compliance at a given point in a structure.

Eq. (4) can be linked to the effective compliance for an element as described below. Suppose that we have some arbitrary, one-dimensional, continuous structure as shown in Fig. 1. Suppose also that the governing equation for the structure can be written as

$$\coprod w(x) = sQ(x) \tag{5}$$

For some location between $x = x_1$ and $x = x_2$ on the structure (see Fig. 1), the mean force associated with the element j described by the coordinates between x_1 and x_2 can be written using the mean value theorem for integrals (Kaplan, 1991):

$$\overline{Q} = \frac{1}{\Delta x}\int_{x_1}^{x_2} Q(x)\,\mathrm{d}x = Q(\hat{x}) \tag{6}$$

where $\overline{Q}$ is the mean force and Δx is the distance between x_1 and x_2. Evaluating Eq. (6) at some point between x_1 and x_2, $\hat{x}$, and substituting for $Q(x)$ using Eq. (5) yields:

$$Q(\hat{x}) = \frac{1}{\Delta x}\frac{1}{s}\int_{x_1}^{x_2} \coprod w(x)\,\mathrm{d}x \tag{7}$$

From Eqs. (6) and (7)

$$s_j = \frac{\int_{x_1}^{x_2} \coprod w(x)\,\mathrm{d}x}{\int_{x_1}^{x_2} Q(x)\,\mathrm{d}x} \tag{8}$$

The factor, s_j, is related to the compliance at the point $\hat{x}$ and can be regarded as the effective compliance of the element j, i.e., the region between x_1 and x_2. The compliance index for the element j can be derived by considering the damaged system subjected to the same force, $Q(x)$. For the damaged system, Eq. (8) can be rewritten as

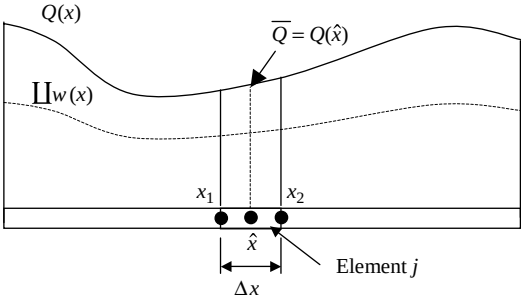

Fig. 1. One-dimensional continuous structural system.

$$s_j^* = \frac{\int_{x_1}^{x_2} \iint w^*(x)\,\mathrm{d}x}{\int_{x_1}^{x_2} Q(x)\,\mathrm{d}x} \tag{9}$$

where the superscript asterisk represents parameters for the damaged system. From Eqs. (8) and (9), the compliance index, β_j^c, which is the ratio of post-damaged compliance to pre-damaged compliance of the element j, can be formulated as follows:

$$\beta_j^c = \frac{s_j^*}{s_j} = \frac{\int_{x_1}^{x_2} \iint w^*\,\mathrm{d}x}{\int_{x_1}^{x_2} \iint w\,\mathrm{d}x} \tag{10}$$

For an arbitrary structural system, the compliance index can be derived in terms of modal vectors as follows. For $i = 1,2,\ldots,N$ sets of modal vectors, Eq. (7) can be rewritten for the jth element as follows:

$$\overline{Q} = Q(\hat{q}_1, \hat{q}_2, \ldots, \hat{q}_n) = \frac{1}{\Delta\Omega_j}\frac{1}{s_j}\int_{\Omega_j} \iint \Phi_i\,\mathrm{d}\Omega \tag{11}$$

where $\hat{q}_1, \hat{q}_2, \ldots, \hat{q}_n$ is the location of the mean force, $\overline{Q}$, in the element j; Ω_j is the domain of the element j and

$$\Delta\Omega_j = \int_{\Omega_j} \mathrm{d}\Omega \tag{12}$$

For a damaged structure, Eq. (11) can be rewritten as

$$\overline{Q} = Q(\hat{q}_1^*, \hat{q}_2^*, \ldots, \hat{q}_n^*) = \frac{1}{\Delta\Omega_j}\frac{1}{s_j^*}\int_{\Omega_j} \iint \Phi_i^*\,\mathrm{d}\Omega \tag{13}$$

Assuming that the change in the mean force is negligible for the pre-damaged and post-damaged elements, a compliance index, β_{ij}^c, may be formulated using Eqs. (11) and (13) as follows:

$$\beta_{ij}^c = \frac{s_j^*}{s_j} = \frac{\int_{\Omega_j} \iint \Phi_i^*\,\mathrm{d}\Omega}{\int_{\Omega_j} \iint \Phi_i\,\mathrm{d}\Omega} \tag{14}$$

Note that the damage index obtained using Eq. (14) is most susceptible to measurement and numerical errors when both numerator and denominator are close to zero. This phenomenon, for example, might be observed at a node of a mode or a support when the element size is very small. In such cases, erroneous damage indices may result in severe localization errors. To avoid this problem, we shift the domain of interest in the problem by adding unity to the denominator and numerator of Eq. (14) (Stubbs et al., 2000):

$$\beta_{ij}^c = \frac{s_j^*}{s_j} = \frac{1 + \int_{\Omega_j} \iint \Phi_i^*\,\mathrm{d}\Omega}{1 + \int_{\Omega_j} \iint \Phi_i\,\mathrm{d}\Omega} \tag{15}$$

For N sets of mode shapes, the following expression will be a convenient form of the composite compliance index:

$$\beta_j^c = \frac{s_j^*}{s_j} = \frac{1 + \sum_{i=1}^{N} \int_{\Omega_j} \iint \Phi_i^*\,\mathrm{d}\Omega}{1 + \sum_{i=1}^{N} \int_{\Omega_j} \iint \Phi_i\,\mathrm{d}\Omega} \tag{16}$$

2.3. Damage localization and severity estimation

Using Eqs. (15) or (16) (Eqs. (1) or (3) for the energy index) as a basis, possible locations of damage in the structure are determined by utilizing various classification algorithms. Based on the magnitude of the

damage index, for each element, a classification algorithm assigns each element into either a damaged or an undamaged category. As presented in a prior study (Stubbs and Garcia, 1996), the classification can be made on the basis of such schemes as (a) Bayes' rule (from which the well-known linear and quadratic discriminant analysis are derived) (Gibson and Melsa, 1975); (b) nearest distance (Nadler and Smith, 1993); and (c) hypothesis testing (Ott, 1993). In this study, hypothesis testing is used for the classification of an element as damaged or not damaged. In hypothesis testing, the alternate hypothesis (H_1) and null hypothesis (H_0) are defined as follows:

H_0: element j of the structure is not damaged.
H_1: element j of the structure is damaged.

To test the hypotheses, the damage indices shown in Eqs. (15) and (16) are standardized using the equation:

$$z_j = \frac{\beta_j - \mu_\beta}{\sigma_\beta} \tag{17}$$

where z_j is the standardized damage index for the jth element; μ_β is the mean of β_j's and σ_β is the standard deviation of β_j's. Assuming that the standardized damage index is normally distributed, a typical probability function of the standardized damage index depicted in Fig. 2 can be used for classification. The following decision rules that correspond to one-tailed test may be used to assign damage to the element j:

(i) choose H_0 if $z_j < z_\eta$, or
(ii) choose H_1 if $z_j \geqslant z_\eta$

where η represents level of significance of the test. The decision making criterion for assigning the location of damage is thus established using elements of statistical decision making. Note that a typical value for the level of significance in damage localization is 0.05 which corresponds to a z score of $z_{0.05} = 1.645$.

Once the possible locations of damage are identified, the corresponding damage severities may be obtained using the corresponding nonstandardized damage indices. Damage severity of an element is defined as the fractional change in stiffness (Park et al., 2001). Since the damage index is the ratio of pre-damaged compliance to post-damaged compliance, the severity of damage for jth element may be expressed as

$$\alpha_j = \frac{k_j^* - k_j}{k_j} = \frac{\frac{1}{s_j^*} - \frac{1}{s_j}}{\frac{1}{s_j}} = \frac{s_j - s_j^*}{s_j^*} = \frac{1}{\beta_j} - 1 \tag{18}$$

Note that the severity (magnitude) of damage obtained using Eq. (18) represents the fractional stiffness loss for a specific element j of the structure.

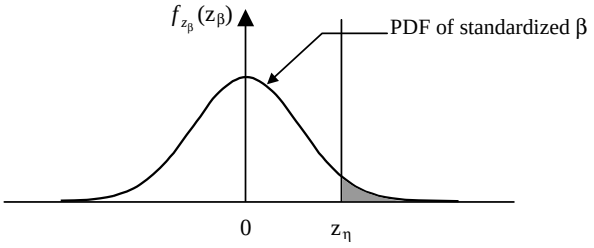

Fig. 2. Probability density functions of standardized damage index.

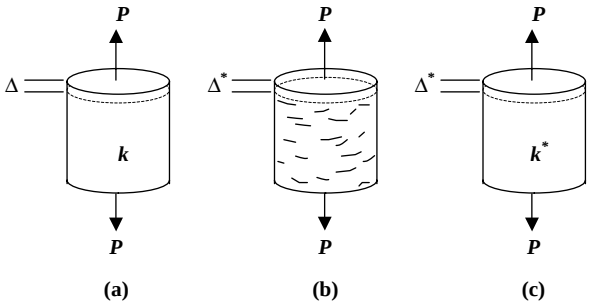

Fig. 3. A rod element subjected to axial loading: (a) undamaged element, (b) damaged element with cracks, (c) damaged element with effective uniform stiffness.

2.4. Concept of effective stiffness

The concept of the effective element compliance increase or stiffness reduction can be demonstrated as follows (Lemaitre and Chaboche, 1990). Considering a rod element with cracks as shown in Fig. 3(b). We may expect significant local stiffness loss in the vicinity of crack and the consequent fluctuation in the compliance or stiffness distribution of the element. Considering a complex structure with many elements, it is not an easy task to determine exact local stiffness loss with limited number of sensors. This problem can be solved by introducing the concept of effective stiffness loss for the element.

Consider a prismatic rod element with the original (pre-damaged) stiffness k as shown in Fig. 3(a). Suppose that the element is subjected to an axial force, P, and the corresponding elongation due to the force P is Δ. Assuming that the rod element is damaged, the elongation due to the same force, P, is changed to Δ^*, as shown in Fig. 3(b). The effective stiffness for the damaged element is the uniform stiffness, k^*, which yields the same elongation as the damaged element subjected to the same axial force. Consider the element with uniform stiffness, k^*, as shown in Fig. 3(c). If the elongation of both the damaged element with cracks (Fig. 3(b)) and the element with uniform stiffness (Fig. 3(c)) are the same for the same axial force, P, then the stiffness, k^*, is the effective stiffness for the damaged element. Thus, the effective reduction in the stiffness of the element due to the introduction of damage is the difference between k and k^*.

3. Numerical verification

3.1. Simply supported beam

The feasibility and performance of the proposed compliance index is first examined via a numerical example of a simply supported beam structure. The example structure is shown in Fig. 4. The beam is equally divided into 36 two-dimensional beam elements as shown in the figure. The length of each element is 0.25 m. All elements are assumed to be made of the same material with $E = 200$ GPa and $\rho = 7827$ kg/m^3. To simulate the actual practice, the responses are assumed to be measured at 13 locations as shown in the figure. The structure is subjected to four damage scenarios in which the number of inflicted damage location ranges from one to three. Damage is numerically simulated by reducing the elastic moduli of the appropriate elements. The locations and corresponding magnitudes of the damage simulated for each damage scenario are summarized in Table 1. Free vibration analysis is performed to obtain mode shapes using SAP2000® (1998). Since to the naked eye the corresponding mode shapes for damaged structures are indistinguishable from undamaged ones, only the mode shapes for the Damage Case 1 are shown in Fig. 5.

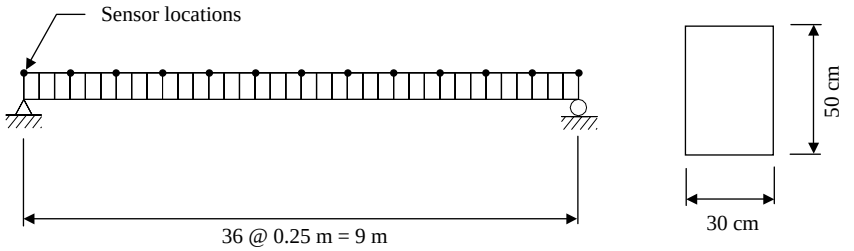

Fig. 4. Simply supported beam.

Table 1
Simulated damage locations and severities

Damage scenario		Elements damaged	Corresponding severity (%)
Simply supported beam	1	24	10
	2	4	50
	3	9, 30	30, 20
	4	4, 21, 31	20, 30, 20
Continuous beam	5	24	10
	6	4	50
	7	21, 40	10, 20
	8	9, 48, 63	20, 30, 30

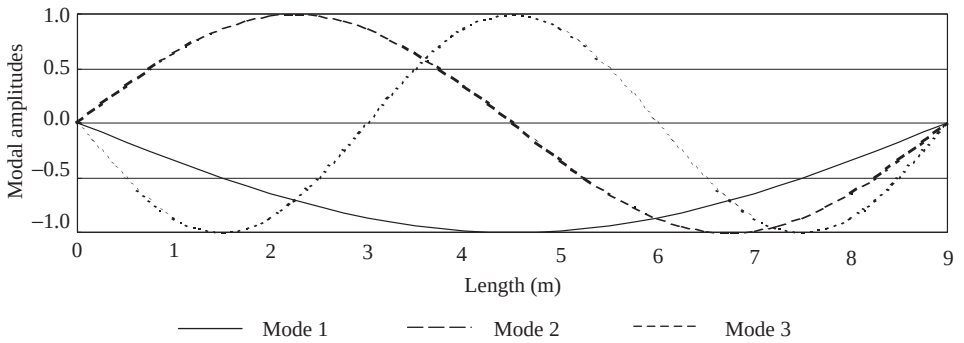

Fig. 5. Mode shapes of the simply supported beam.

3.2. Continuous beam

A continuous two span beam is used here to further verify numerically the effectiveness of the compliance index. The section and material properties are the same as the simply supported beam. The model has 72 elements and 73 nodes, as shown in Fig. 6. Again, to simulate the actual practice, the responses are assumed to be measured at 25 locations. The structure is subjected to four damage scenarios. The locations and corresponding magnitudes of the damage simulated for each damage scenario are also summarized in Table 1. The mode shapes of the structure are shown in Fig. 7.

3.3. Measurement noise

In the field application of modal testing to obtain the mode shapes, it is expected that there would be some deviations due to measurement noise. To simulate this condition, a series of random noise generated

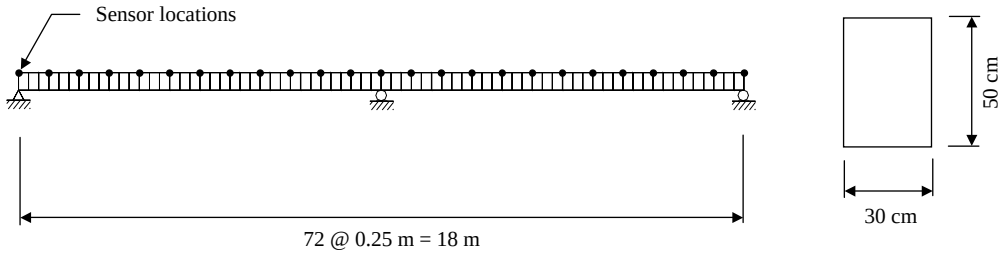

Fig. 6. Continuous beam.

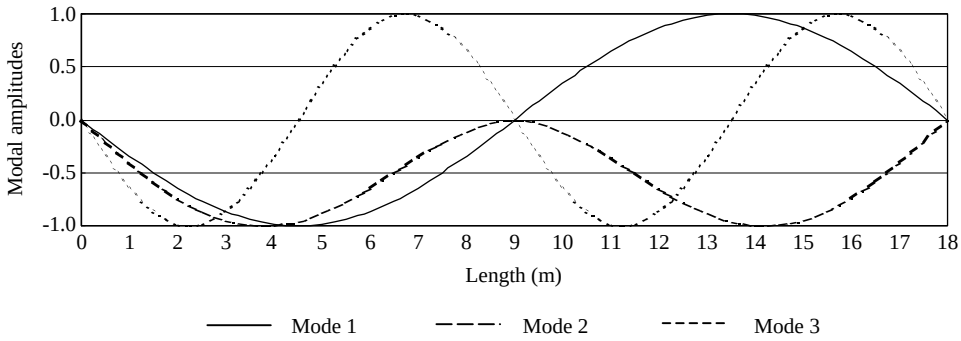

Fig. 7. Mode shapes of the continuous beam.

from a uniform distribution on the interval $[-1, 1]$ is added to the original mode shapes of the structure. The degree of noise is determined by a noise/signal (NS) ratio that is a ratio of the random-number series to the amplitude of the mode shape. In present applications, the effect of different level of noise on damage identification is investigated by applying 0.1% and 1% NS ratios.

3.4. Damage localization and severity estimation

Using the proposed compliance indices expressed in Eqs. (15) and (16), the determination of the locations of potential damage in the structure is implemented using the following steps. First, the damage index for each element is calculated using Eqs. (15) and (16). Second, the obtained damage indices are standardized using Eq. (17). Third, the presence of damage in Element j is determined according to the pre-assigned classification rules: (a) the element is damaged if $z_j \geqslant 1.5$; (b) the element is not damaged if $z_j < 1.5$. Note that the value of the damage indicator, 1.5, corresponds to a 93% confidence level for the presence of damage. Next, the severity of damage for possible damage location is estimated as follows. First, the possible damage elements are identified using the hypothesis testing algorithm. Second, the severities of those elements are estimated using Eq. (18). Also, for comparison the same calculation is performed using the energy index presented in Eqs. (1) and (3).

3.5. Discussion of results

The damage localization results are shown in Figs. 8–15. In all of the figures, note that the inflicted locations of damage are indicated by the tilted arrows. The vertical axis is in the nondimensional unit of the standardized damage index for that particular location. Note also that only the damage localization results

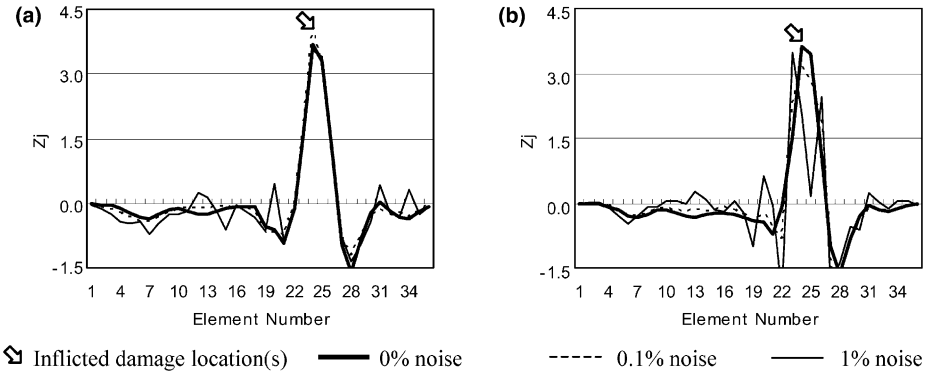

Fig. 8. Damage localization results of Damage Case 1 for the simply supported beam: (a) compliance index, (b) energy index.

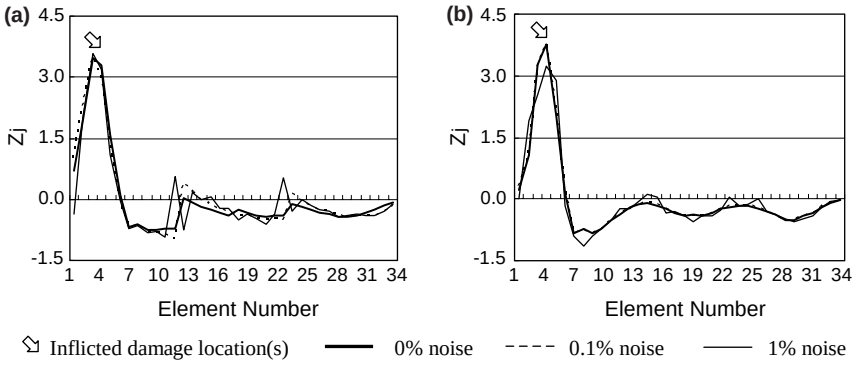

Fig. 9. Damage localization results of Damage Case 2 for the simply supported beam: (a) compliance index, (b) energy index.

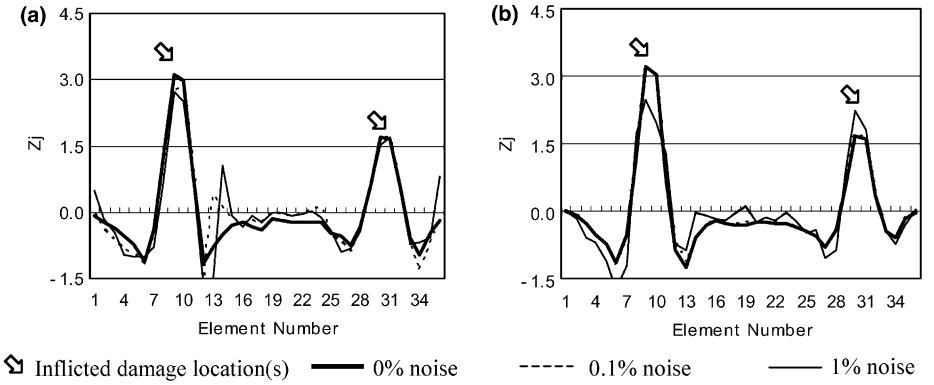

Fig. 10. Damage localization results of Damage Case 3 for the simply supported beam: (a) compliance index, (b) energy index.

using the composite damage index are presented due to space limitation. The percentage of false positive prediction (Type I error) and the percentage of false negative prediction (Type II error) are used to evaluate the performance of the methodology. A false positive means that damage is reported where no damage

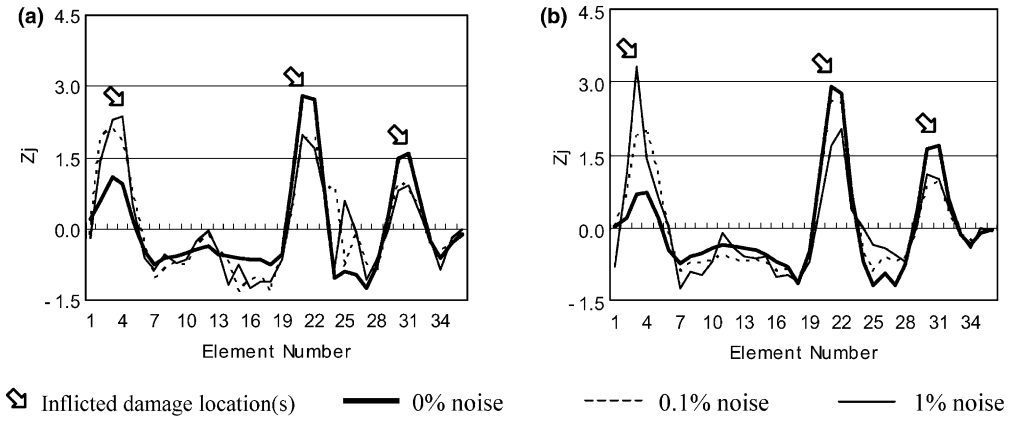

Fig. 11. Damage localization results of Damage Case 4 for the simply supported beam: (a) compliance index, (b) energy index.

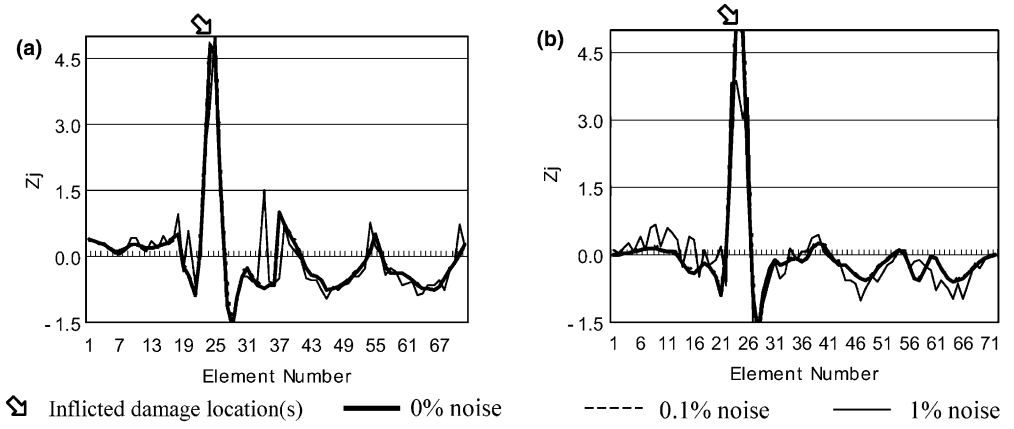

Fig. 12. Damage localization results of Damage Case 5 for the continuous beam: (a) compliance index, (b) energy index.

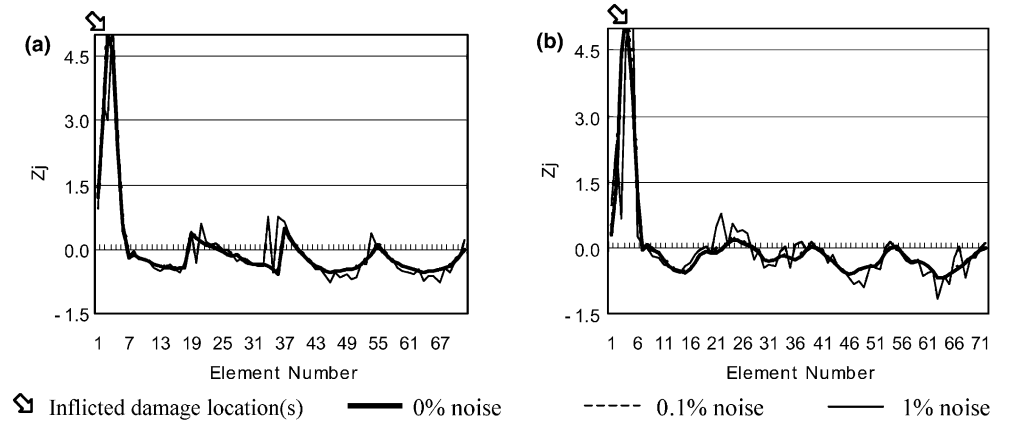

Fig. 13. Damage localization results of Damage Case 6 for the continuous beam: (a) compliance index, (b) energy index.

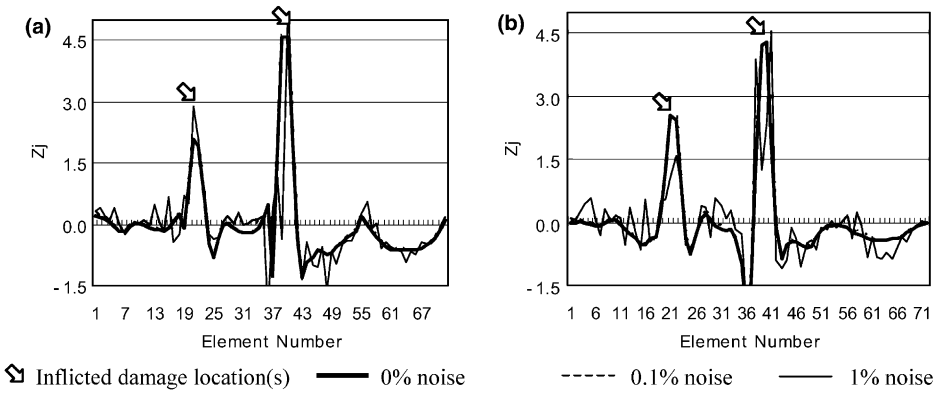

Fig. 14. Damage localization results of Damage Case 7 for the continuous beam: (a) compliance index, (b) energy index.

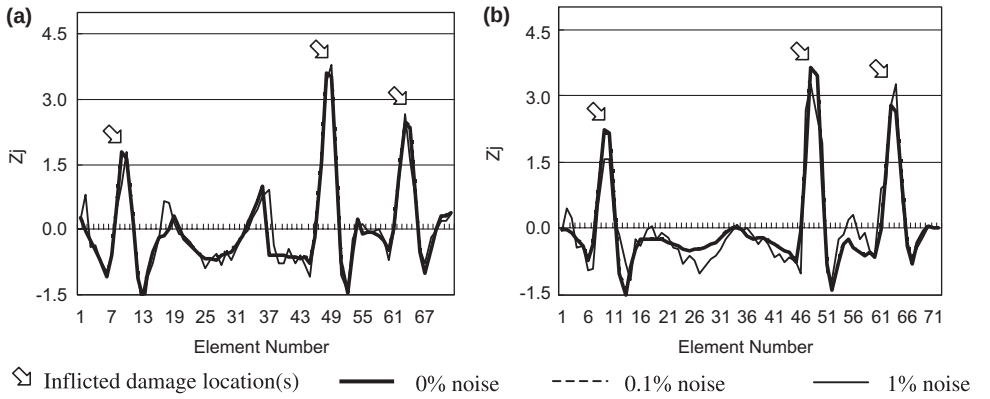

Fig. 15. Damage localization results of Damage Case 8 for the continuous beam: (a) compliance index, (b) energy index.

exists and a false negative means that damage is not reported where damage exists. The percentage of false positive error is calculated by dividing the number of false positive predictions by the number of undamaged elements, and the percentage of false negative error is calculated by dividing the number of false negative predictions by the number of damaged elements. In an ideal situation, the false positive and the false negative error rates should be zero. In the present application, the consequence of a false negative is much greater than that of a false positive. The false positive and the false negative may reflect the quality of the measured data and the effectiveness of damage localization algorithm. The number and resulting percentage of false positives and false negatives for each damage case are summarized in Tables 2 and 3, respectively. Note that in the tables, the performance of the method is evaluated using the individual modes (i.e., Mode 1, Mode 2, and Mode 3) as well as the combined one (i.e., 3 Modes).

For damage cases with a single damage location that correspond to Damage Cases 1, 2, 5, and 6, the proposed compliance index based method successfully identifies all simulated damage locations (zero false negatives) with noise free data (see Table 3). A few false positives are observed but all the false positive predictions arise in the neighborhood of the simulated damage locations. For the same damage cases with noise, the method again identifies all damage locations except Mode 2 in Damage Case 5 when 1% noise is introduced. In the damage localization results for damage cases with multiple damage locations, Damage

Table 2
Number of false positives

Damage case	Mode 1			Mode 2			Mode 3			3 Modes		
	0%[a]	0.1%	1%	0%	0.1%	1%	0%	0.1%	1%	0%	0.1%	1%
1	2	2	1	1	1	1	3	2	2	2	2	2
	(2)	(3)	(2)	(1)	(1)	(2)	(3)	(3)	(2)	(2)	(3)	(2)
2	3	3	1	3	3	3	2	2	2	3	2	2
	(2)	(3)	(1)	(2)	(2)	(1)	(2)	(2)	(3)	(2)	(2)	(3)
3	2	2	0	1	2	1	3	2	2	2	2	2
	(1)	(1)	(2)	(1)	(1)	(3)	(2)	(2)	(2)	(2)	(2)	(3)
4	1	1	1	3	3	3	2	1	2	1	3	2
	(1)	(1)	(1)	(1)	(2)	(2)	(2)	(1)	(2)	(2)	(1)	(2)
5	3	3	3	3	3	3	2	2	3	3	3	4
	(3)	(3)	(2)	(7)	(8)	(2)	(3)	(3)	(3)	(3)	(3)	(3)
6	3	3	2	3	3	2	3	3	3	3	3	3
	(2)	(3)	(2)	(2)	(3)	(2)	(2)	(2)	(4)	(2)	(3)	(2)
7	5	4	4	2	2	2	3	3	3	4	3	2
	(3)	(2)	(2)	(2)	(3)	(3)	(3)	(2)	(2)	(3)	(4)	(3)
8	4	4	3	4	4	4	4	4	3	4	4	3
	(4)	(3)	(5)	(4)	(5)	(4)	(3)	(3)	(5)	(4)	(4)	(5)
$\sum$	23	22	15	20	21	20	22	19	20	22	22	20
	(18)	(19)	(17)	(20)	(25)	(19)	(20)	(18)	(23)	(20)	(22)	(23)
%	5.50	5.26	3.59	4.78	5.02	4.78	5.26	4.55	4.78	5.26	5.26	4.78
	(4.31)	(4.55)	(4.07)	(4.78)	(5.98)	(4.55)	(4.78)	(4.31)	(5.50)	(4.78)	(5.26)	(5.50)

( ) Results using the energy index.
[a] NS ratio.

Table 3
Number of false negatives

Damage case	Mode 1			Mode 2			Mode 3			3 Modes		
	0%[a]	0.1%	1%	0%	0.1%	1%	0%	0.1%	1%	0%	0.1%	1%
1	0	0	0	0	0	0	0	0	0	0	0	0
	(0)	(0)	(1)	(0)	(0)	(0)	(1)	(1)	(1)	(0)	(0)	(0)
2	0	0	0	0	0	0	0	0	0	0	0	0
	(0)	(0)	(0)	(0)	(0)	(0)	(0)	(0)	(0)	(0)	(0)	(0)
3	1	1	0	0	1	1	0	1	0	0	0	0
	(1)	(1)	(1)	(1)	(1)	(0)	(0)	(0)	(0)	(0)	(0)	(0)
4	2	3	2	1	2	2	1	1	1	1	1	1
	(2)	(2)	(3)	(2)	(2)	(3)	(1)	(1)	(1)	(1)	(1)	(2)
5	0	0	0	0	0	1	0	0	0	0	0	0
	(0)	(0)	(0)	(0)	(0)	(1)	(0)	(0)	(0)	(0)	(0)	(0)
6	0	0	0	0	0	0	0	0	0	0	0	0
	(0)	(0)	(0)	(0)	(0)	(0)	(0)	(0)	(0)	(0)	(0)	(0)
7	0	0	0	1	1	1	0	0	0	0	0	0
	(1)	(1)	(1)	(1)	(1)	(2)	(1)	(1)	(1)	(0)	(0)	(1)
8	0	0	1	0	0	0	1	1	1	0	0	1
	(0)	(1)	(2)	(1)	(1)	(1)	(0)	(0)	(0)	(0)	(0)	(0)
$\sum$	3	4	3	2	4	5	2	3	2	1	1	2
	(4)	(5)	(8)	(5)	(5)	(7)	(3)	(3)	(3)	(1)	(1)	(3)
%	21.4	28.6	21.4	14.3	28.6	35.7	14.3	21.4	14.3	7.1	7.1	14.3
	(28.6)	(35.7)	(57.1)	(35.7)	(35.7)	(50.0)	(21.4)	(21.4)	(21.4)	(7.1)	(7.1)	(21.4)

( ) Results using the energy index.
[a] NS ratio.

Cases 3, 4, 7, and 8, the method performs quite satisfactorily with noise-free data. A few false positives are observed, but all damage locations occur at the vicinity of the inflicted damage locations as shown in Figs. 8–15. When noise added, the percentage of false negative shows a tendency to increase as the NS ratio increases. However, even with the severest simulated noise level (NS ratio = 1%), most of damage locations can be inferred from the localization results (see Figs. 8 and 9). From Table 2, the percentage of false positives seems not to be influenced significantly by increasing the number of damage locations and the noise level. As expected, in Tables 2 and 3, better damage identification results are obtained using the composite damage indices which simultaneously include the information of all three modes. One notable result is that the more reliable and accurate damage localization results could be obtained using the proposed compliance index than the existing energy index. In the tables, it is observed that the compliance index yields similar false positives but smaller false negatives than the energy index.

Another way to evaluate the performance of the proposed compliance index is as follows. In all 8 damage cases a total of 14 damage sites are inflicted. Without noise, the composite compliance index unambiguously locates 13 of these 14 cases. This result corresponds to an overall success rate of 93%. For reference, the composite form of the existing energy index yields the same success rate. When noise is added,

Table 4
Severity estimation results

Damage case		Mode 1			Mode 2			Mode 3			3 Modes		
		0%[a]	0.1%	1%	0%	0.1%	1%	0%	0.1%	1%	0%	0.1%	1%
1	0.1[b]	0.04	0.03	0.02	0.03	0.03	0.02	0.02	0.02	0.00	0.03	0.03	0.01
		(0.04)	(0.01)	–	(0.03)	(0.03)	(0.01)	–	–	–	(0.04)	(0.02)	(0.00)
2	0.5	0.25	0.23	0.11	0.25	0.24	0.18	0.23	0.23	0.29	0.23	0.23	0.24
		(0.28)	(0.28)	(0.04)	(0.27)	(0.26)	(0.20)	(0.25)	(0.25)	(0.10)	(0.26)	(0.25)	(0.12)
3	0.3	0.14	0.13	0.07	0.10	0.11	0.15	0.08	0.08	0.07	0.09	0.09	0.09
		(0.14)	(0.13)	(0.05)	(0.11)	(0.11)	(0.07)	(0.09)	(0.09)	(0.06)	(0.11)	(0.11)	(0.06)
	0.2	–	–	0.03	0.05	–	–	0.05	–	0.05	0.05	0.05	0.04
		–	–	–	–	–	(0.05)	(0.06)	(0.06)	(0.05)	(0.06)	(0.06)	(0.04)
4	0.2	–	–	–	–	0.72	0.35	–	–	–	–	0.09	0.12
		–	–	–	–	(0.03)	–	–	–	–	–	(0.13)	–
	0.3	0.12	–	0.21	0.11	–	–	0.09	0.10	0.09	0.09	0.09	0.09
		(0.13)	(0.14)	–	–	–	–	(0.10)	(0.10)	(0.11)	(0.12)	(0.11)	(0.07)
	0.2	–	–	–	0.06	–	–	0.05	0.06	0.06	0.06	–	–
		–	–	–	(0.07)	–	–	(0.07)	(0.07)	(0.07)	(0.07)	–	–
5	0.1	0.04	0.04	0.02	0.03	0.07	–	0.03	0.03	0.03	0.04	0.04	0.02
		(0.04)	(0.04)	(0.02)	(0.03)	(0.55)	–	(0.04)	(0.04)	(0.02)	(0.04)	(0.04)	(0.02)
6	0.5	0.26	0.21	0.08	0.25	0.21	0.08	0.25	0.26	0.30	0.25	0.24	0.17
		(0.28)	(0.17)	(0.02)	(0.27)	(0.14)	(0.01)	(0.29)	(0.30)	(0.33)	(0.29)	(0.22)	(0.04)
7	0.1	0.03	0.04	0.20	–	–	–	0.03	0.04	0.06	0.03	0.03	0.06
		(0.04)	(0.04)	(0.00)	–	–	–	–	–	–	(0.04)	(0.04)	–
	0.2	0.08	0.07	0.03	0.08	0.08	0.20	0.07	0.07	0.06	0.07	0.07	0.07
		–	–	–	(0.09)	(0.09)	–	(0.07)	(0.06)	(0.01)	(0.08)	(0.08)	(0.01)
8	0.2	0.08	0.11	–	0.09	0.08	0.06	–	–	–	0.05	0.05	–
		(0.08)	–	–	(0.09)	(0.08)	(0.02)	(0.05)	(0.05)	(0.04)	(0.07)	(0.07)	(0.03)
	0.3	0.13	0.12	0.09	0.12	0.11	0.09	0.11	0.11	0.10	0.11	0.11	0.10
		(0.13)	(0.13)	(0.08)	–	–	–	(0.13)	(0.13)	(0.07)	(0.13)	(0.13)	(0.07)
	0.3	0.07	0.07	0.05	0.07	0.08	0.12	0.06	0.07	0.09	0.07	0.07	0.09
		(0.07)	(0.07)	–	(0.07)	(0.08)	(0.15)	(0.09)	(0.09)	(0.08)	(0.08)	(0.08)	(0.07)

( ) Results using the energy index.
[a] NS ratio.
[b] Simulated damage.

the method identifies 13 and 12 in 14 simulated damage locations using the composite damage index, which corresponds to a success rate of 93 and 86%, respectively. In case of the energy index, the success rate gets little worse with 93% and 76%.

The severity estimation results using the compliance index and the energy index are presented in Table 4. For all damage cases, the compliance index consistently yields lower damage severity estimates than the simulated values. The fact that damage is smeared into the neighboring elements, as shown in Figs. 8–15, may explain this systematic error. In the table, it is also observed that the compliance index gives a reasonable agreement between damage magnitudes using the noise-free and the noise-polluted data. The same phenomena are observed in the results using the energy index.

4. Experimental verification

4.1. Description of experiment

The proposed method is further verified using the experimental data from a free–free beam. The 1.91 cm (3/4 in.) diameter circular bar with the length of 61 cm (24 in.) is used as the test specimen. In order to simulate the free–free boundary condition, two 18 gauge wires approximately 61 cm in length were used. Fig. 16 shows the test beam and the measurement locations. The accelerometer was attached at Location 3 and damage was inflicted at Location 5. In this study, Location 1 corresponds to $x = 0$ cm, Location 2 corresponds to $x = 10.2$ cm (4 in.), and so on. A hacksaw was used to introduce the intended damage to the specimen. Note that an ordinary hacksaw approximately 0.5 mm (0.02 in.) in width was used to cut a groove in the surface of the beam specimen and the depth of the groove was measured using a ruler. To verify the detectability, three levels of damage severity, saw cut depth of 3.175 mm (1/8 in.), 6.35 mm (1/4 in.) and 9.525 mm (3/8 in.) were inflicted on the specimen, respectively. The damage scenarios and the corresponding defects are summarized in Table 5.

Fig. 17 depicts the equipments utilized in this test. The equipments consisted of a 4-channel Digital Signal Processor (DSP), an impact hammer, a piezoelectric accelerometer and a personal computer (PC) equipped with Siglab software (1996). The DSP and Siglab software, designated model 20-42, were manufactured by the Signal Analysis Group. The impact hammer was a Piezotronics (PCB) model 086C01. The accelerometer utilized in the experiment was a PCB model 303A03. Test settings used for the modal test are summarized in Table 6.

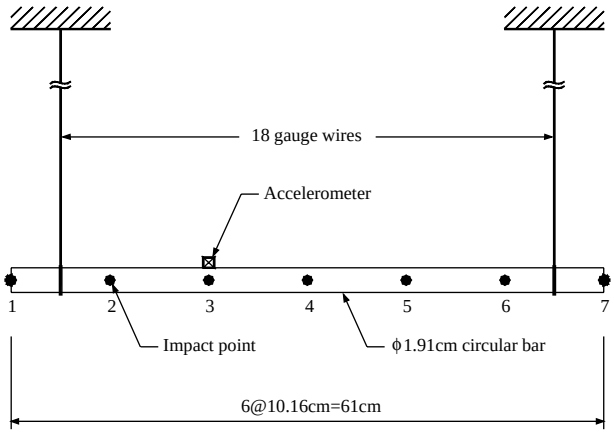

Fig. 16. A free–free beam.

Table 5
Damage scenarios and corresponding defects

Damage scenario	Description
1	3.175 mm deep saw cut at $x = 40.6$ cm (16 in.)
2	6.350 mm deep saw cut at $x = 40.6$ cm (16 in.)
3	9.525 mm deep saw cut at $x = 40.6$ cm (16 in.)

Fig. 17. Test equipments.

Table 6
Modal test parameters for the test

Parameter	Setting	Notes/units
Sample frequency	5000	Hz
Sample length	8192	Samples per channel
Spectral resolution	0.61	Hz
Number of repetitions	3	Linear average
Channel gain	Varied	Set to maximize resolution
Trigger method	+18% Hammer FS	Pre-trigger save all channels
Accelerometer window	Exponential	99% Down at end
Hammer window	Rectangular	7% Window width

4.2. Result and discussion

The modal parameters were obtained from the plot of frequency response function using the commercial software (Siglab, 1996). Four resonant frequencies and corresponding mode shapes were extracted for each state of the specimens (see Table 7 and Fig. 18). Using the extracted mode shapes and the damage indices in

Table 7
Natural frequencies of the test beam

Frequency mode	Undamaged case (Hz)	Damage scenario 1 (Hz)	Damage scenario 2 (Hz)	Damage scenario 3 (Hz)
1	234.38	232.19	231.25	228.13
2	640.63	637.50	631.25	618.75
3	1251.56	1250.00	1250.00	1248.44
4	2053.13	2048.44	2042.19	2020.31

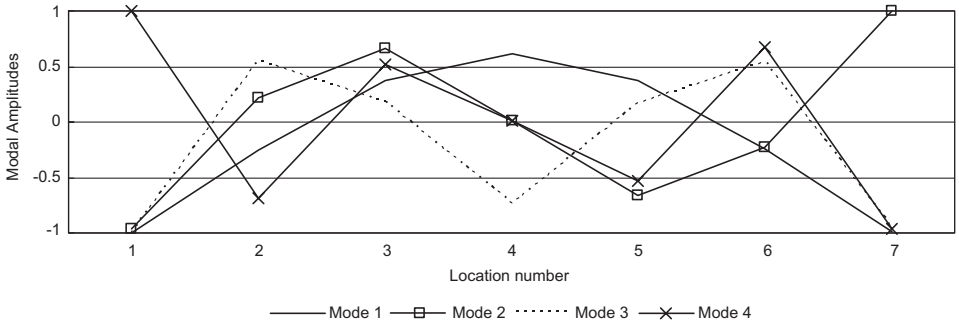

Fig. 18. Mode shapes of the test free–free beam.

Eq. (3) for the energy index and Eq. (16) for the compliance index, the identification of defects on the specimens is implemented using the following steps. First, the damage detection model for damage identification is built. The model has 49 elements and 50 nodes. The modal amplitudes for nodes between the impact points are interpolated using the cubic spline function (Press et al., 1992). Note that the location of damage corresponds to Element 33. Second, the damage index for each element in the damage detection model is calculated applying the identified four mode shapes to Eqs. (3) and (16). Third, the obtained damage indices are standardized using Eq. (17). Finally, the presence of defect in Element j is determined according to the pre-assigned classification rules: the element is damaged if $z_j \geqslant 1.5$; or the element is not damaged if $z_j < 1.5$. Note that the severity estimation results are not compared in this example since the exact quantitative estimation of the hacksaw-inflicted damage to the element of the specimen is almost impossible.

Fig. 19 presents the graphical representation of the damage identification results using the compliance index and the energy index. In the figure, the followings are observed. In the damage identification result for Damage Case 1, both the compliance index and the energy index successfully identified the inflicted damage. In the damage identification result for Damage Case 2, the strain energy index gives better indication of the presence of damage than the compliance index. However, in the damage identification result for Damage Case 3, the strain energy index does not identify the location of damage while the compliance index does. This shows the better sensitivity of the compliance index to damage and the advantage of having the alternative damage predictions for a certain locations in the structure. In the figure, the solid lines without marks represent the average value of the two damage indices calculated as follows:

$$\beta_{\text{average}} = \sum_{i=1}^{NM} \left[\beta_i^{\text{c}} + \beta_i^{\text{e}}\right] \tag{19}$$

It can be observed that the average of the two indices give damage predictions without identification error in all damage scenarios.

5. Summary and conclusions

In this paper, a methodology to locate and size damage in a structure using a new type of damage index was presented. The new damage index, here designated as the compliance index, utilized the changes in the distribution of the compliance of a structure due to damage. The change in the compliance distribution was obtained using the changes in the mode shapes of a structure due to damage. The concept of the compliance index along with the effective compliance was presented in this paper. The validity of the methodology was

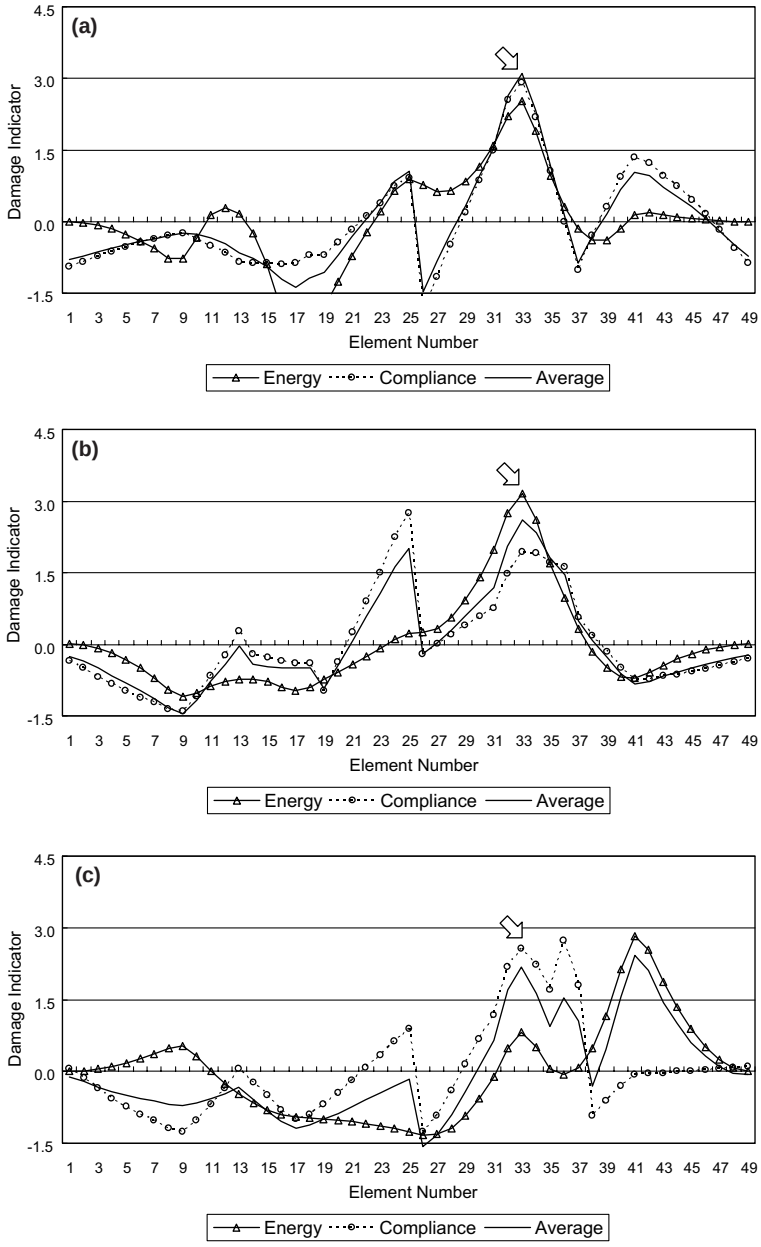

Fig. 19. Damage identification results for the test beam. (a) Damage case 1, (b) Damage Case 2, (c) Damage Case 3.

demonstrated using data from numerical examples of beam structures and the results were compared with those using the existing energy index. The experimental verification was also performed using data from the free–free beam structure. In three damage cases, the proposed compliance index identified all damage locations while the energy index failed to identify damage in one damage case. Also, it is observed that the average of the two indices give damage predictions without identification error in all damage scenarios.

From the results obtained in the study, the following conclusions are drawn:

1. the compliance index based on the change in the effective compliance change of an element of a structure can be used for damage localization and severity estimation;
2. the numerical and experimental studies reveal that the compliance index can identify single and multiple damage locations consistently and accurately;
3. the compliance index yields less damage identification error that the existing energy index;
4. performance of damage localization and severity estimation may be improved by using the composite damage indices which utilize multiple mode shapes simultaneously;
5. the compliance and energy indices consistently produced a lower damage severity estimations and
6. in the experimental study, the average of the two indices, i.e., the compliance and the energy indices, gives damage predictions without identification error in all three damage scenarios.

References

Askeland, D.R., 1994. The Science and Engineering of Materials. PWS Publishing Company, USA.

Cawley, P., Adams, R.D., 1979. The location of defects in structures from measurements of natural frequencies. Journal of Strain Analysis 14 (2), 49–57.

Choi, S., Stubbs, N., 1997. Nondestructive damage detection algorithms for 2d plates. Smart Structures and Materials 1997: smart systems for bridges, structures, and highways. SPIE Proceedings 3043, 193–204.

Choi, S., Stubbs, N., 2004. Damage identification in structures using the time domain response. Journal of Sound and Vibration 275 (3–5), 577–590.

Choi, S., Park, S., Bolton, R., Stubbs, N., Sikorsky, C., 2004. Periodic monitoring of physical property changes in a concrete box-girder bridge. Journal of Sound and Vibration 278 (1–2), 365–381.

Doebling, S.W., Farrar, C.R., Prime, M.B., Shevitz, D.W., 1996. Damage identification and health monitoring of structural and mechanical systems from changes in their vibrational characteristics: a literature review. Technical Report LA-13070-MS, Los Alamos National Laboratory.

Farrar, C., Jauregui, D., 1996. Damage detection algorithms applied to experimental and numerical modal data from the I-40 bridge. Technical Report LA-13074-MS, Los Alamos National Laboratory, 1996.

Gibson, J.D., Melsa, J.L., 1975. Introduction to Nonparametric Detection with Applications. Academic Press, USA.

Gudmundson, P., 1982. Eigenfrequency changes of structures due to cracks, notches, or other geometrical changes. Journal of Mechanics and Physics of Solids 30 (5), 339–353.

Kaplan, W., 1991. Advanced Calculus. Addison-Wesley, USA.

Kim, J.T., Stubbs, N., 1995. Model-uncertainty impact and damage-detection accuracy in plate girder. Journal of Structural Engineering 121 (10), 1409–1417.

Ko, J.M., Sun, Z.G., Ni, Y.Q., 2002. Multi-stage identification scheme for detecting damage in cable-stayed Kap Shui Mun Bridge. Engineering Structures 24, 857–868.

Lemaitre, J., Chaboche, J.-L., 1990. Mechanics of Solid Materials. Cambridge University Press, USA.

Lu, Q., Ren, G., Zhao, Y., 2002. Multiple damage location with flexibility curvature and relative frequency change for beam structures. Journal of Sound and Vibration 253 (5), 1101–1114.

Nadler, M., Smith, E.P., 1993. Pattern Recognition Engineering. John Wiley & Sons, USA.

Ott, R.L., 1993. An Introduction to Statistical Methods and Data Analysis. Wadsworth Inc, USA.

Pandey, A.K., Biswas, M., 1994. Damage detection in structures using changes in flexibility. Journal of Sound and Vibration 169 (1), 3–17.

Pandey, A.K., Biswas, M., 1995. Experimental verification of flexibility difference method for locating damage in structures. Journal of Sound and Vibration 184 (2), 311–328.

Pandey, A.K., Biswas, M., Samman, M.M., 1991. Damage detection from changes in curvature mode shapes. Journal of Sound and Vibration 145 (2), 321–332.

Park, S., Stubbs, N., Bolton, R., Choi, S., Sikorsky, C., 2001. Field verification of the damage index method in a concrete box-girder bridge via visual inspection. Computer-Aided Civil and Infrastructure Engineering 16, 58–70.

Press, W.H., Teukosky, S.A., Vetterling, W.T., Flannery, B.P., 1992. Numerical Recipes in FORTRAN. Cambridge University Press, USA.

Rizos, P.F., Aspragathos, N., Dimarogonas, A.D., 1990. Identification of crack location and magnitude in a cantilever beam from the vibration modes. Journal of Sound and Vibration 138 (3), 381–388.

Rodriguez, R., 2002. Stiffness–mass ratios method for baseline determination and damage assessment of a benchmark structure. M.S. thesis, Texas A&M University, USA.

SAP2000®, 1998. User's Manual. Computers and Structures, USA.

Siglab User's Guide, vol. 1. Fremont, California. Signal Analysis Group, 1996.

Stubbs, N., Garcia, G., 1996. Application of pattern recognition to damage localization. Microcomputers in Civil Engineering 11, 395–409.

Stubbs, N., Kim, J.T., Topole, K.G., 1992. An efficient and robust algorithm for damage localization in offshore platforms. ASCE 10th Structures Congress, pp. 543–546.

Stubbs, N., Park, S., Sikorsky, C., Choi, S., 2000. A global nondestructive damage assessment methodology for civil engineering structures. International Journal of Systems Science 31 (11), 1361–1373.

Vandiver, J.K., 1977. Detection of structural failure on fixed platforms by measurement of dynamic response. Journal of Petroleum Technology, 305–310.

Zhang, Z., Aktan, H.M., 1995. The damage indices for the constructed facilities. Proceedings of IMAC 13 (2), 1520–1529.

Zimmerman, D.C., Kaouk, M., 1994. Structural damage detection using a minimum rank update theory. ASME Journal of Vibration and Acoustics 116, 222–231.